ISSN 2435-2640

Proceedings of the School of Science of Tokai University

Vol. 57, Mar. 2022

東海大学紀要
理学部

PUBLISHED BY
SCHOOL OF SCIENCE, TOKAI UNIVERSITY
TOKYO, JAPAN

東海大学紀要

理 学 部

Vol. 57, Mar. 2022

目　次

Proceedings of the School of Science of Tokai University

CONTENTS

Vol. 57, Mar. 2022

Proc. Sch. Sci. TOKAI UNIV.
57 (2022) 1–10
DOI: 10.18995/24352640.57.1

Adsorption of Decylpyridinium Iodide on Aqueous Surfaces of Sodium Iodide Solutions

by

Katsuhiko Fujio*[1] and Kazuhiro Orihara[2]

[1]*Department of Chemistry, School of Science, Tokai University*
4–1–1 Kitakaname, Hiratsuka-shi, Kanagawa, 259–1292, Japan
[2]*Department of Chemistry, Faculty of Science, Shinshu University*
3–1–1 Ashahi, Matsumoto-shi, Nagano, 390–8621, Japan
*Corresponding author: E-mail: kfujio@tokai-u.jp
(Received on Oct. 22, 2021; accepted on Dec. 6, 2021)

Abstract

We have measured the surface tension of aqueous NaI solutions of decylpyridinium iodide (DePI) by the drop weight method at different NaI concentrations from 0 to 80 mmol dm^{-3} at 25℃ and obtained surface excess densities of decylpyridinium ion (DeP^+), I^- and Na^+ as functions of DePI concentration at different NaI concentrations by applying the Gibbs adsorption isotherm to the surface tension data at DePI concentrations below the critical micelle concentration (CMC). Surface excess densities of DeP^+ and I^- increase with increasing DePI concentration, and approach the saturated values at the CMC excluding the most concentrated NaI solution. On the other hand, the surface excess density of Na^+ is nearly zero or slightly negative. The molecular area of DePI on aqueous surface increases with increasing NaI concentration up to 5 mmol dm^{-3} and then decreases, as associated with very small micelles of DePI in the absence of NaI. The Corrin-Harkins plot is linear in NaI concentration range studied, which suggests DePI forms only spherical micelles.

Keywords: decylpyridinium iodide; surface tension; Langmuir adsorption; critical micelle concentration

1 Introduction

Surfactant molecules or ions are adsorbed on aqueous surface and consequently lower the surface tension of their aqueous solutions. Using the Gibbs adsorption isotherm, Equations (2) – (4), we can obtain the surface excess densities of nonionic surfactant molecule and concomitant salt from the dependence of surface tension on concentrations of surfactant and salt.

In the case of ionic surfactant in aqueous salt solution, however, only these equations are not sufficient to evaluate the surface excess densities of surfactant ion, counterion and constituent ions of salt. Ikeda and coworkers [1–7] derived the surface excess densities of surfactant ion

and all other ionic species as functions of concentrations of surfactant and concomitant salt in terms of the Gibbs adsorption isotherm and applied them to some alkylammonium surfactant-sodium halide systems; dodecyldimethylammonium chloride (DDAC)-NaCl [2, 3], dodecyldimethylammonium bromide (DDAB)-NaBr [4], DDAC-NaBr [5], hexadecyltrimethylammonium bromide (CTAB)-NaBr [6], DDAB-NaCl [7] and dodecyltrimethylammonium bromide (DTAB)-NaBr [8].

Cationic surfactants with a quaternary ammonium head group are fully ionized over whole practical pH range and adsorbed onto most solid-water interface, which are usually negatively charged, so that they have special applications such as water-repellent and antistatic agents [9]. Furthermore, they exhibit good bactericidal action and hence for example hexadecylpyridinium bromide are used in mouthwashes [10]. Factors affecting these properties of cationic surfactants including alkylpyridinium halides are interesting. In the previous work [11, 12], therefore, we extended similar measurements of surface tension to aqueous NaCl solutions of dodecylpyridinium and tetradecylpyridinium chlorides (DPC and TPC) having an aromatic ring as a polar head group, and determined the surface excess densities of dodecylpyridinium and tetradecylpyridinium ions (DP^+ and TP^+), Cl^- and Na^+ as functions of surfactant and NaCl by applying the Gibbs adsorption isotherm according to Ikeda and coworkers [1–7]. As observed for other cationic surfactant-simple salt systems, surface excess densities of DP^+, TP^+ and Cl^- increased with increasing surfactant concentration and approached the saturated values at the critical micelle concentration (CMC), whereas the surface excess density of Na^+ was nearly zero or slightly negative. Like common ionic surfactants, the molecular area of TPC on aqueous surface decreased with increasing NaCl concentration except for $0\,\mathrm{mol\,dm^{-3}}$ NaCl solution. On the other hand, that of DPC increased with increasing NaCl concentration up to $0.010\,\mathrm{mol\,dm^{-3}}$ and then decreased to almost constant value, as explained by the formation of very small micelles of DPC below 0.05 $\mathrm{mol\,dm^{-3}}$ NaCl.

In the present work we study the adsorption behavior of decylpyridinium iodide (DePI), whose hydrophilic tail is the shorter by two methylene groups than DPC and whose counterion is different from that of surfactants studied previously, on aqueous surfaces of NaI solutions in order to investigate the effect of alkyl chain length and the influence of the kind of counterion on the adsorption of alkylpyridinium halide on aqueous surfaces of sodium halide solutions.

2 Experimental

DePC was synthesized by refluxing the mixture of pyridine and 1-iododecane at 120℃ for 7 hours and recrystallized three times from acetone-diethyl ether mixture (1:2 v/v). Pyridine was obtained from Nacalai Tesque, Inc., and dried over molecular sieves 3A. 1-iododecane was purchased from ACROS ORGANICS and used without purification. NaI of special grade reagent from Nacalai Tesque, Inc., was dried at 120℃ for two hours. Water was redistilled from alkaline $KMnO_4$ solution.

The surface tension of aqueous solutions was measured at 25 ± 0.1℃ by the drop weight method. A capillary having a reservoir was kept perpendicular in a glass vessel immersed in a temperature-controlled bath and its upper end was connected to a micrometer syringe through a rubber tube. We suspended a drop of solution at the lower end of capillary in a state just before falling for 5 min or more, and then detached it from the capillary tip. If a drop which falls from the capillary

tip having outer radius r has a weight m, then the surface tension of the solution is given by

$$\gamma = \frac{mg}{r} F \tag{1}$$

where g is the gravitational acceleration and F is the Harkins-Brown correction factor determined by the drop volume V and the outer radius r of the tip. The drop volume V was obtained by dividing the drop weight m by the density of solvent, i.e., water or NaI solution. The effective outer radius r of the capillary tip was determined by measuring the drop weight of redistilled water and assuming its surface tension to be 71.98 $\mathrm{mN\,m^{-1}}$ and found to be 3.457 mm. The capillary was cleaned by being immersed in chromic acid mixture after each measurement.

3 Results

Figure 1 shows the surface tension, γ, of aqueous NaI solutions of DePI plotted against the logarithm of the molar concentration of DePI, $\log C$, at different NaI concentrations, C_S. As the DePI concentration increases up to the CMC, the surface tension decreases and its rate of decrease increases from about zero to a certain definite value. Above the CMC, the surface tension has an almost constant value at a given NaI concentration. Surface tension is lower at the higher NaI concentration unless the DePI concentration is very low. The concentration dependence of surface tension of the DePI-NaI system is similar to that of DPC- and TPC-NaCl systems [11, 12] and alkylammonium surfactant-sodium halide systems [2–8]. Table 1 gives the CMC, C_0, and the surface tension at the CMC, γ_0. Both quantities decrease with increasing NaI concentration.

According to the Gibbs adsorption isotherm, the surface tension depression can be represented by

$$-\mathrm{d}\gamma = RT\,(\Gamma \mathrm{d}\ln C + \Gamma_\mathrm{S} \mathrm{d}\ln C_\mathrm{S}) \tag{2}$$

where R is the gas constant and T is the absolute temperature. Γ and Γ_S are the surface excess

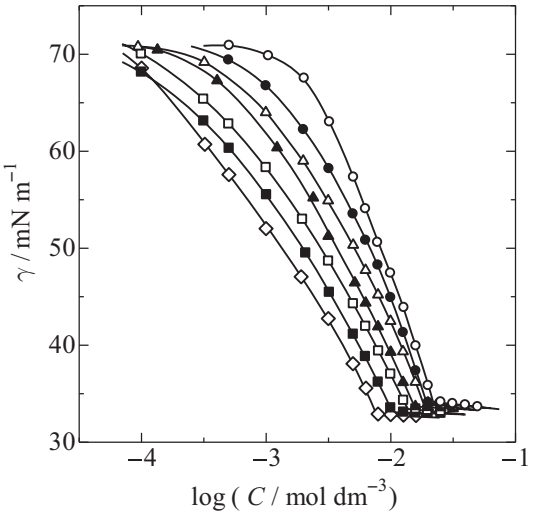

Fig. 1 Dependence of surface tension of aqueous NaI solutions of DePI on surfactant concentration at different NaI concentrations. C_S / $\mathrm{mmol\,dm^{-3}}$: ○, 0; ●, 5; △, 10; ▲, 20; □, 30; ■, 50; ◇, 80.

Table 1 Adsorption properties of DePI on the surface of aqueous NaI solution at the CMC, C_0.

C_S / mmol dm^{-3}	C_0 / mmol dm^{-3}	γ_0 / mN m^{-1}	Γ / 10^{-6} mol m^{-2}	Γ_S / 10^{-6} mol m^{-2}
0	21.8	34.2	7.76	
5.00	19.4	34.0	6.92	1.16
10.01	18.3	34.0	5.93	1.10
20.02	15.5	33.7	4.98	1.81
30.03	13.7	33.4	4.58	1.84
50.12	10.3	33.1	4.55	2.61
80.23	7.7	32.8	5.23	2.73

densities of DePI and NaI, respectively, defined by

$$\Gamma = -\frac{1}{RT}\left(\frac{\partial\gamma}{\partial \ln C}\right)_{C_S} \tag{3}$$

and

$$\Gamma_S = -\frac{1}{RT}\left(\frac{\partial\gamma}{\partial \ln C_S}\right)_{C} \tag{4}$$

Γ can be evaluated from the slope of curves shown in Figure 1.

In order to estimate Γ_S, the surface tension is plotted afresh against the logarithm of the NaI concentration, log C_S, at each DePI concentration, C, as shown in Figure 2. This figure also indicates the NaI concentration dependence of surface tension at the CMC, γ_0, by a dashed line.

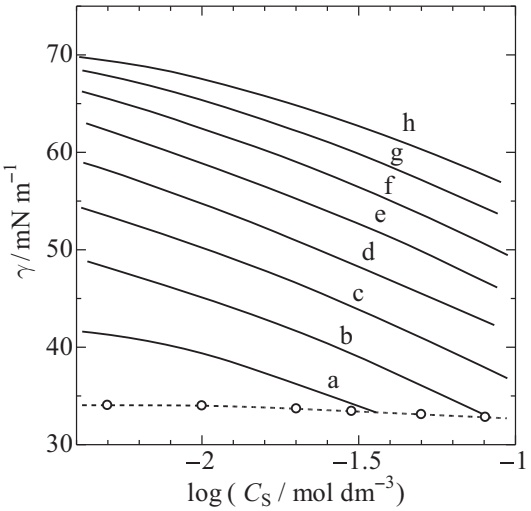

Fig. 2 Dependence of surface tension of aqueous NaI solutions of DePI on NaI concentration at different DePI concentrations. –log (C / mol dm^{-3}): a, 1.9; b, 2.1; c, 2.3; d, 2.5; e, 2.7; f, 2.9; g, 3.1; h, 3.3. Dashed curve represents dependence of surface tension at the CMC, γ_0, on NaI concentration.

Table 1 also includes values of Γ and Γ_S at the CMC. With increasing NaI concentration the value of Γ at the CMC decreases, has a minimum value at 50.12 mmol dm^{-3} NaI and then increases. The value of Γ_S at the CMC also exhibits the similar NaI concentration dependence with a minimum at 10.01 mmol dm^{-3} NaI. Excluding the decrease in Γ_S at low NaI concentration, such behavior of Γ and Γ_S at the CMC has been observed for DPC- and TPC-NaCl systems [11, 12] and alkylammonium surfactant-sodium halide systems [3–8].

4 Discussion

4.1 Surface excess densities of ions

According to Ikeda and coworkers [1–7], the Gibbs adsorption isotherm can be applied to the surface tension data at DePI concentrations below the CMC, shown in Figures 1 and 2, and the surface excess densities of decylpyridinium ion (DeP^+), I^- and Na^+ can be determined as functions of DePI and NaI concentrations. Furthermore, their works [2, 3] indicated that the substitution of activities of surfactant and salt by their molar concentrations causes no serious errors in calculations of surface excess densities for such systems containing a dilute ionic surfactant and a simple salt.

Representing the surface excess densities subject to the Gibbs convention of DeP^+, I^- and Na^+ by Γ_{DeP^+}, Γ_{I^-} and Γ_{Na^+}, respectively, the coefficients, Γ and Γ_S, in the Gibbs adsorption isotherm, Equation (2), can be represented by

$$\Gamma = \left(1 + \frac{C}{C + C_S}\right)\Gamma_{DeP^+} + \frac{C}{C + C_S}\Gamma_{Na^+} \tag{5}$$

and

$$\Gamma_S = \frac{C_S}{C + C_S}\Gamma_{DeP^+} + \left(1 + \frac{C_S}{C + C_S}\right)\Gamma_{Na^+} \tag{6}$$

respectively [2, 3]. Solving these equations for Γ_{DeP^+} and Γ_{Na^+}, the following equations can be obtained:

$$\Gamma_{DeP^+} = \frac{1}{2}\left\{\left(1 + \frac{C_S}{C + C_S}\right)\Gamma - \frac{C}{C + C_S}\Gamma_S\right\} \tag{7}$$

and

$$\Gamma_{Na^+} = \frac{1}{2}\left\{-\frac{C_S}{C + C_S}\Gamma + \left(1 + \frac{C}{C + C_S}\right)\Gamma_S\right\} \tag{8}$$

The electroneutrality of the surface gives the surface excess density of I^- in the following form:

$$\Gamma_{I^-} = \Gamma_{DeP^+} + \Gamma_{Na^+} = \frac{1}{2}(\Gamma + \Gamma_S) \tag{9}$$

Applying Equations (7) – (9) to the surface tension data given in Figures 1 and 2, the surface excess densities of three ionic species below the CMC can be obtained. Figures 3 and 4 show the surface excess density of DeP^+ and those of I^- and Na^+, respectively, at different NaI concentrations as functions of DePI concentration.

With increasing DePI concentration, the value of Γ_{DeP^+} increases towards a saturated value except for the most concentrated NaI solution. It appears that above 20.02 mmol dm^{-3} NaI the value of Γ_{DeP^+} is already saturated at the low DePI concentrations.

The value of Γ_{Na^+} is nearly zero or slightly negative except the case of 5.00 mmol dm^{-3} NaI, where it is slightly positive. Consequently, the value of Γ_{I^-} is nearly equal to that of Γ_{DeP^+}.

Table 2 gives Γ_{DeP^+}, Γ_{I^-} and Γ_{Na^+} at the CMC for different NaI concentrations and Figure 5 shows them plotted against the square root of the NaI concentration.

Figure 6 plots $1/\Gamma_{DeP^+}$ smaller than 0.6×10^6 m^2 mol^{-1}, above which small values of Γ_{DeP^+} cause significant errors in calculating $1/\Gamma_{DeP^+}$, against $1/C$ and gives straight lines at each NaI concentration. This indicates that the adsorption of DeP^+ obeys the Langmuir isotherm

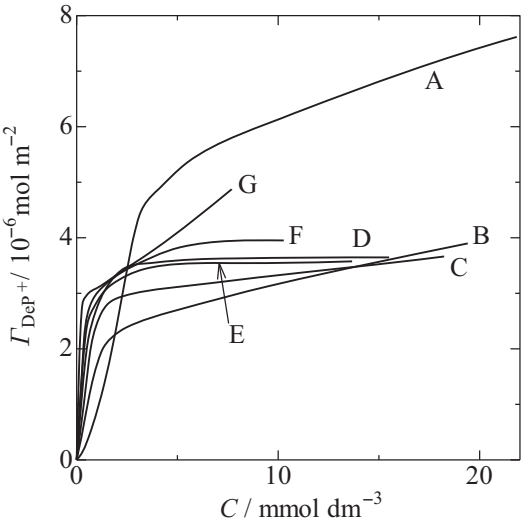

Fig. 3 Adsorption isotherm of decylpyridinium ion, DeP^+, on aqueous surface at different NaI concentrations. C_S / mmol dm^{-3}: A, 0; B, 5; C, 10; D, 20; E, 30; F, 50; G, 80.

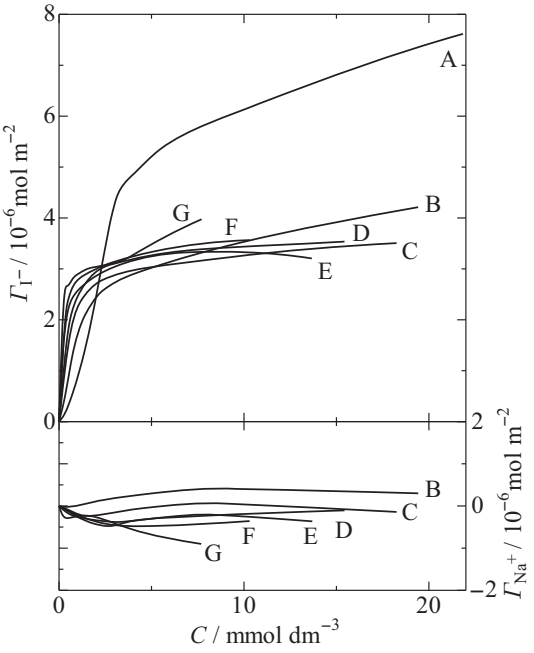

Fig. 4 Adsorption isotherms of I^- (upper) and Na^+ (bottom) on aqueous surface at different NaI concentrations. C_S / mmol dm^{-3}: A, 0; B, 5; C, 10; D, 20; E, 30; F, 50; G, 80.

Table 2 Surface excess densities of decylpyridinium ion, I^- and Na^+ at the CMC.

C_S / mmol dm^{-3}	Γ_{DeP^+} / 10^{-6} mol m^{-2}	Γ_{I^-} / 10^{-6} mol m^{-2}	Γ_{Na^+} / 10^{-6} mol m^{-2}
0	7.76	7.76	
5.00	3.71	4.04	0.33
10.01	3.66	3.51	−0.14
20.02	3.50	3.39	−0.10
30.03	3.57	3.21	−0.36
50.12	3.94	3.58	−0.36
80.23	4.88	3.98	−0.90

$$\Gamma_{DeP^+} = \Gamma^{\infty}_{DeP^+} \frac{KC}{1+KC} \tag{10}$$

where $\Gamma^{\infty}_{DeP^+}$ is the saturated adsorption density of DeP^+ and K is the adsorption coefficient. Table 3 gives values of $\Gamma^{\infty}_{DeP^+}$ and K at different NaI concentrations.

The molecular area, A_0, corresponding to $\Gamma^{\infty}_{DeP^+}$ is obtained in Å^2 by

$$A_0 = \frac{10^{20}}{N_A \Gamma^{\infty}_{DeP^+}} \tag{11}$$

where N_A is the Avogadro constant, and its values are also given in Table 3. The molecular area of common ionic surfactant such as DTAB decreases with increasing salt concentration because the electrostatic shielding effect of salt weakens the electrostatic repulsion between the charged head groups of the adsorbed surfactant ions [8]. With increasing NaI concentration, however, the molecular area of DePI increases from 21.7 Å^2 in the absence of NaI to 51.9 Å^2 at 5.00 mmol dm^{-3}

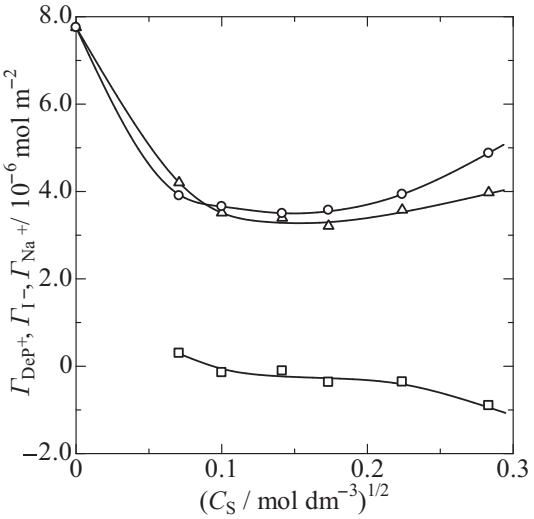

Fig. 5 Dependence of surface excess densities of decylpyridinium ion, I^- and Na^+ at the CMC on NaI concentration. ○, Γ_{DeP^+}; △, Γ_{I^-}; □, Γ_{Na^+}.

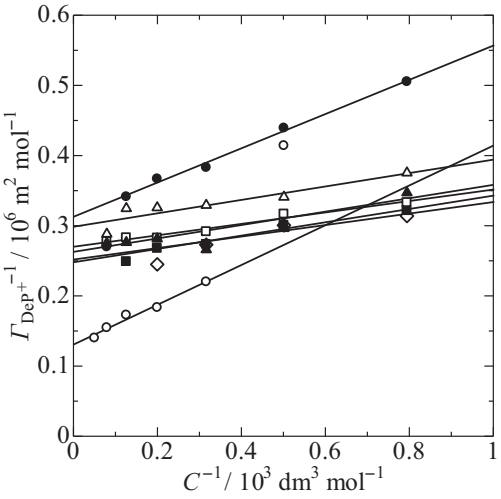

Fig. 6 Langmuir isotherm of decylpyridinium ion at different NaI concentrations. C_S / mmol dm^{-3}: ○, 0; ●, 5; △, 10; ▲, 20; □, 30; ■, 50; ◇, 80.

Table 3 Saturated adsorption density, molecular area, adsorption coefficient and free energy of adsorption of DePI.

C_S / mmol dm^{-3}	$\Gamma^{\infty}_{DeP^+}$ / 10^{-6} mol m^{-2}	A_0 / Å^2	K / 10^3 dm^3 mol^{-1}	ΔG_{ad} / kJ mol^{-1}
0	7.66	21.7	0.46	−15.2
5.00	3.20	51.9	1.28	−17.7
10.01	3.35	49.6	3.12	−19.9
20.02	3.84	43.2	2.46	−19.4
30.03	3.70	44.8	3.29	−20.1
50.12	3.84	43.2	3.92	−20.5
80.23	3.76	44.1	5.02	−21.1

NaI, and then decreases to about 44 Å^2 at 20.02 mmol dm^{-3} NaI, above which the molecular area remains almost constant. Similar dependence of molecular area on salt concentration was observed for DPC-NaCl system: with increasing NaCl concentration, the molecular area of DPC increased from 28.9 Å^2 in the absence of NaCl to 63.5 Å^2 at 0.010 mol dm^{-3} NaCl, and then decreased to almost constant value of 55 Å^2 above 0.050 mol dm^{-3} NaCl [11]. This dependence of molecular area of DPC on NaCl concentration was inferred to be associated with very small micelles of DPC in aqueous NaCl solution below 0.05 mol dm^{-3} [13]. The NaI concentration dependence of molecular area of DePI also would be interpreted in the same manner.

Table 3 shows that the adsorption coefficient K increases with increasing NaI concentration, which suggests the electrostatic shielding effect of NaI on the adsorption of DeP^+, except for 20.02 mol dm^{-3} NaI. This exception would be attributed to a large error in K due to a deviation of the $1/\Gamma_{DeP^+}$ vs. $1/C$ plot from a straight line expected by the Langmuir isotherm.

Table 3 also includes values of the free energy of adsorption evaluated from K by

$$\Delta G_{ad} = -RT \ln K \tag{12}$$

Corresponding to the increase in K, ΔG_{ad} decreases with NaI concentration except for the case of 20.02 mmol dm^{-3} NaI.

K and ΔG_{ad} for the DePI-NaI system are compared with those for DPC- and TPC-NaCl systems at the same salt concentrations in Table 4. The free energy of adsorption is the smallest for TPC and is almost same for DePI and DPC, but slightly smaller for DePI than for DPC. In the previous study the smaller free energy of adsorption of TPC than DPC was explained by the dominant role of the hydrophobic effect of the alkyl chain in the adsorption of surfactant ions [12]. In this case the higher counterion binding of I^- to a charged self-assembly such as micelle than Cl^- [14] also would have to be considered. The higher counterion binding results in the smaller free energy of adsorption because the electrostatic repulsion between head groups of adsorbed surfactants is weakened.

Table 4 Adsorption coefficient and free energy of adsorption of DePI, DPC and TPC.

C_{S} / mol dm^{-3}		DePI	DPC [11]	TPC [12]
0	K / dm^3 mol^{-1}	461	350	638
	ΔG_{ad} / kJ mol^{-1}	−15.2	−14.5	−16.0
0.01	K / dm^3 mol^{-1}	3120	1900	27600
	ΔG_{ad} / kJ mol^{-1}	−19.9	−18.7	−25.3
0.05	K / dm^3 mol^{-1}	3920	3800	82200
	ΔG_{ad} / kJ mol^{-1}	−20.5	−20.4	−28.1

4.2 Critical micelle concentration

The CMC of DePI decreases with increasing NaI concentration, as given in Table 1. It follows the Corrin-Harkins equation

$$\log\left(C_0/\mathrm{mol\,dm^{-3}}\right) = -0.734 \log\left\{\left(C_0 + C_{\mathrm{S}}\right)/\mathrm{mol\,dm^{-3}}\right\} - 2.88 \qquad (13)$$

as shown in Figure 7.

For DDAB-NaBr and DTAB-NaBr systems, the Corrin-Harkins plot consists of two linear plots

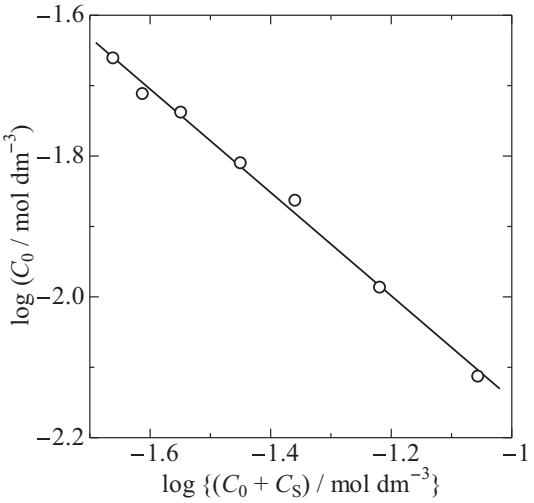

Fig. 7 The Corrin-Harkins plot of DePI in aqueous NaI solutions.

at low and high NaBr concentrations owing to the salt-induced sphere-rod transition of their micelles [15, 16]. The slope of Corrin-Harkins plot for DePI can be compared with those for DDAB [4] and DTAB [8] at low NaBr concentrations, where spherical micelles are formed:

$$\log\left(C_0/\mathrm{mol\,dm^{-3}}\right) = -0.452\log\left\{\left(C_0+C_\mathrm{S}\right)/\mathrm{mol\,dm^{-3}}\right\} - 2.83 \tag{14}$$

and

$$\log\left(C_0/\mathrm{mol\,dm^{-3}}\right) = -0.674\log\left\{\left(C_0+C_\mathrm{S}\right)/\mathrm{mol\,dm^{-3}}\right\} - 3.04 \tag{15}$$

and those for DPC [11], where only spherical micelle is formed [13], and TPC [12]:

$$\log\left(C_0/\mathrm{mol\,dm^{-3}}\right) = -0.684\log\left\{\left(C_0+C_\mathrm{S}\right)/\mathrm{mol\,dm^{-3}}\right\} - 2.98 \tag{16}$$

and

$$\log\left(C_0/\mathrm{mol\,dm^{-3}}\right) = -0.679\log\left\{\left(C_0+C_\mathrm{S}\right)/\mathrm{mol\,dm^{-3}}\right\} - 3.99 \tag{17}$$

Consequently, the Corrin-Harkins plot suggests DePI forms only spherical micelles.

As the CMC is a good measure of stability of the micellar state relative to the monomeric state, Equations (13) – (17) indicates that the stability of DePI micelles is lower than that of DDAB, DTAB, DPC and TPC micelles.

5 Conclusion

By applying the Gibbs adsorption isotherm to the surface tension of aqueous NaI solutions of DePI at 25℃, surface excess densities of DeP^+, I^- and Na^+ have been derived as functions of DePI concentration at different NaI concentrations. As observed for other cationic surfactant-simple salt systems, surface excess densities of DeP^+ and I^- increase with increasing DePI concentration and approach the saturated values at the CMC except for the most concentrated NaI solution, whereas the surface excess density of Na^+ is nearly zero or slightly negative. The molecular area of DePI on aqueous surface increases with increasing NaI concentration up to 5.00 $\mathrm{mmol\,dm^{-3}}$ and then decreases. This might be associated with very small micelles of DePI in the absence of NaI. The Corrin-Harkins plot is linear in NaI concentration range studied, which suggests DePI forms only spherical micelles. The free energy of adsorption for DePI-NaI system is slightly smaller than that for DPC-NaCl system, as explained by competition between the hydrophobic effect of alkyl chain and the counterion binding to adsorbed surfactant film.

References

[1] S. Ikeda, *Hyomen*, **15**, 592 (1977).

[2] S. Ozeki, M. Tsunoda and S. Ikeda, *J. Colloid Interface Sci.*, **64**, 28 (1978).

[3] S. Ozeki and S. Ikeda, *Bull. Chem. Soc. Jpn.*, **53**, 1832 (1980).

[4] H. Okuda, S. Ozeki and S. Ikeda, *Bull. Chem. Soc. Jpn.*, **57**, 1321 (1984).

[5] H. Okuda, S. Ozeki and S. Ikeda, *J. Colloid Interface Sci.*, **115**, 155 (1987).

[6] H. Okuda, T. Imae and S. Ikeda, *Colloids Surf.*, **27**, 187 (1987).

[7] H. Okuda and S. Ikeda, *J. Colloid Interface Sci.*, **131**, 333 (1989).

[8] A. Tanaka and S. Ikeda, *Colloids Surf.*, **56**, 217 (1991).

[9] J. C. Berg, "An Introduction to Interfaces and Colloids: The Bridge to Nanoscience", World Scientific, New Jersey, 2010, chap. 3.

[10] M. J. Rosen and J. T. Kunjappu, "Surfactants and Interfacial Phenomena", 4th Ed., John Wiley & Sons, New Jersey, 2012, chap. 1.

[11] K. Fujio, K. Takeuchi and M. Suzuki, *Proc. Sch. Sci. Tokai Univ.* , **47**, 35 (2012).

[12] K. Fujio, K. Hayashi and M. Suzuki, *Proc. Sch. Sci. Tokai Univ.*, **49**, 55 (2014).

[13] K. Fujio and S. Ikeda, *Bull. Chem. Soc. Jpn.*, **65**, 1406 (1992).

[14] K. Fujio and S.Ozeki, *J. Japan Oil Chem. Soc.*, **49**, 221 (2000).

[15] S. Ozeki and S. Ikeda, *Colloid Polym. Sci.*, **262**, 409 (1984).

[16] S. Ozeki and S. Ikeda, *J. Colloid Interface Sci.*, **87**, 424 (1982).

Proc. Sch. Sci. TOKAI UNIV.
57 (2022) 11–17
DOI: 10.18995/24352640.57.11

Influence of relative humidity on the behavior of aerosols generated from heated tobacco products

by

Takumi YAMAMOTO[1], Yoshika SEKINE*[2], Koki SOHARA[3],
Satoshi NAKAI[4] and Yukio YANAGISAWA[5]

[1]*Course of Chemistry, Graduate School of Science, Tokai University*
4–1–1 Kitakaname, Hiratsuka, Kanagawa, 259–1292 Japan
[2]*Department of Chemistry, School of Science, Tokai University, Kanagawa, Japan*
4–1–1 Kitakaname, Hiratsuka, Kanagawa, 259–1292 Japan
[3]*Graduate School of Earth and Environmental Sciences, Tokai University*
4–1–1 Kitakaname, Hiratsuka, Kanagawa, 259–1292 Japan
[4]*Graduate School of Environment and Information Sciences, Yokohama National University,*
79–7 Tokiwadai, Hodogaya, Yokohama, Kanagawa 240–8501, Japan
[5]*Professor Emeritus, The University of Tokyo*
*Corresponding author: E-mail: sekine@keyaki.cc.u-tokai.ac.jp
(Received on Oct. 22, 2021; accepted on Dec. 6, 2021)

Abstract

Heated tobacco products are devices that deliver nicotine into the body via inhalation of the mainstream aerosols generated during direct and/or indirect heating of tobacco leaf material. These aerosols consist primarily of "water droplets" that contain glycerin and/or propylene glycol as an aerosol former, and thus these hygroscopic aerosols will gain or lose water until reaching an equilibrium with the moisture content in the surrounding atmosphere. In this study, we sought to determine the influence of relative humidity (RH) on the behavior of the aerosols generated from a "low-temperature type" device in a test chamber (0.57 m^3). Concentrations of $PM_{2.5}$ and PM_{10} after puffing were measured using a smartphone air quality monitor, based on a laser light scattering method, under low RH (29%) and high RH (82%) conditions. The results revealed that the levels of $PM_{2.5}$ and PM_{10} in air, along with size distribution and decay rates, were highly dependent on test chamber RH.

Keywords: Aerosol, Relative humidity, Glycerin, Propylene glycol, Heated tobacco products

1 Introduction

Heated tobacco products, also referred to as heat-not-burn tobacco products, are battery-operated devices that deliver nicotine into the body via inhalation of the mainstream aerosol gen-

erated during the direct and/or indirect heating of tobacco leaf material [1–4]. This novel medium is being promoted as a less hazardous alternative to conventional cigarettes for both smokers and non-smokers, given that the tobacco leaf is heated without burning to generate nicotine-containing aerosols, and thus eliminates the emission of side-stream smoke [1–4]. However, considering the chemical and physical properties of aerosols, the potential adverse health effects of these products should be carefully investigated.

The mainstream aerosol generated by these devices consists primarily of "water droplets," which contain glycerin and/or propylene glycol that functions as an aerosol former [5], and thus is fundamentally different in origin and chemical and physical composition when compared with conventional cigarette smoke [5, 6]. Given that glycerin and propylene glycol are hygroscopic in nature, owing to the presence of hydroxyl groups in their molecules, the generated aerosol gains or loses water until reaching an equilibrium with the moisture content in the surrounding atmosphere [7]. Consequently, it is necessary to gain a better understanding of aerosol deposition in the respiratory system and indoor environments for assessing the potential health effects on both active and passive smokers.

The mainstream aerosol exhaled by smokers can be a source of particulate matter (PM) in air. To assess the PM produced by heated tobacco products, Nakai et al. [8] generated a mainstream aerosol from commercially available heated tobacco products in the laboratory and measured the concentrations of $PM_{2.5}$ (fine particulate matter with a size of 2.5 μm or less) in indoor air using an optical $PM_{2.5}$ monitor in responses to changing the temperature of the sensor unit from 21℃ to 45℃. They found that the measured $PM_{2.5}$ concentrations decreased with an increase in the temperature of the sensor unit, owing to an accelerated evaporation of the hygroscopic aerosol by heat. To date, however, the influence of relative humidity (RH) on PM concentrations in indoor air has not been investigated. Accordingly, in this study, we sought to determine the influence of RH on the behavior of hygroscopic aerosols in air contained within a test chamber.

2 Methods

2.1 Heated tobacco product

The Ploom TECH (JT Inc., Tokyo, Japan) device used for the purposes of this study was purchased from a retail tobacco store in Japan. The device consists of a rechargeable battery, cartridge, and consumable tobacco capsule. A "Mevius regular" was used as the tobacco capsule in this study. The aerosol is generated by heating liquid in the cartridge containing aerosol formers and passing this through the tailor-made tobacco capsule at approximately 30°C. This device is thus categorized as a "low-temperature-type" device, in contrast to other brands, such as IQOS (PMI Inc., USA) and glo (BAT, UK), which are classed as "high-temperature-type" devices.

2.2 Experimental setup

Fig. 1 shows the experimental setup used in this study. The mainstream aerosol was generated from the Ploom TECH device using an LM4E Linear Vaping Machine for E-cigarettes (Borgwaldt KC, GmbH, Germany). The outlet port of the vaping machine was connected to a test chamber ($0.57\,m^3$) constructed from acrylic boards with a short silicone tube. Thus, the generated aerosol

was directly introduced with puffing into the test chamber. The dimensions of the chamber were 1.34 m (height) × 0.85 m (width) × 0.50 m (depth). Laboratory air was constantly introduced into the chamber using two diaphragm pumps. When changing the RH in the chamber, laboratory air was passed through pure water (Milli-Q, Millipore Corporation, USA, resistivity=18 MΩ·cm) contained in the impingers. The air within the chamber was thoroughly mixed by a small fan operated continuously at a constant rate. The air exchange rate was determined to be 2.2 h^{-1}, as measured based on the CO_2 tracer gas decay method. The temperature and RH were monitored using a TR-72U thermo recorder (T and D, Tokyo, Japan), and concentrations of $PM_{2.5}$ and PM_{10} (fine particulate matter with a size of 10 μm or less) were measured using a smartphone air quality monitor (Pocket $PM_{2.5}$ sensor; Yaguchi Electric Corporation, Miyagi, Japan), which employs a laser light scattering method for the detection of $PM_{2.5}$ and PM_{10}. The monitor consists of a laser light-emitting diode, photodiode sensor, fan, amplifier, and USB encoder connected to an Android-type smartphone [9, 10]. The smartphone displays $PM_{2.5}$ and PM_{10} concentrations in units of μg m^{-3}, and the background screen color changes from blue to yellow, red, purple, and black with an increase in PM levels. The monitor also generates log data expressed as comma-separated values of the Google Keyhole Markup Language format, including the global positioning system. The calibrated monitors used in this study were purchased from the IDEC Corporation (Tokyo, Japan).

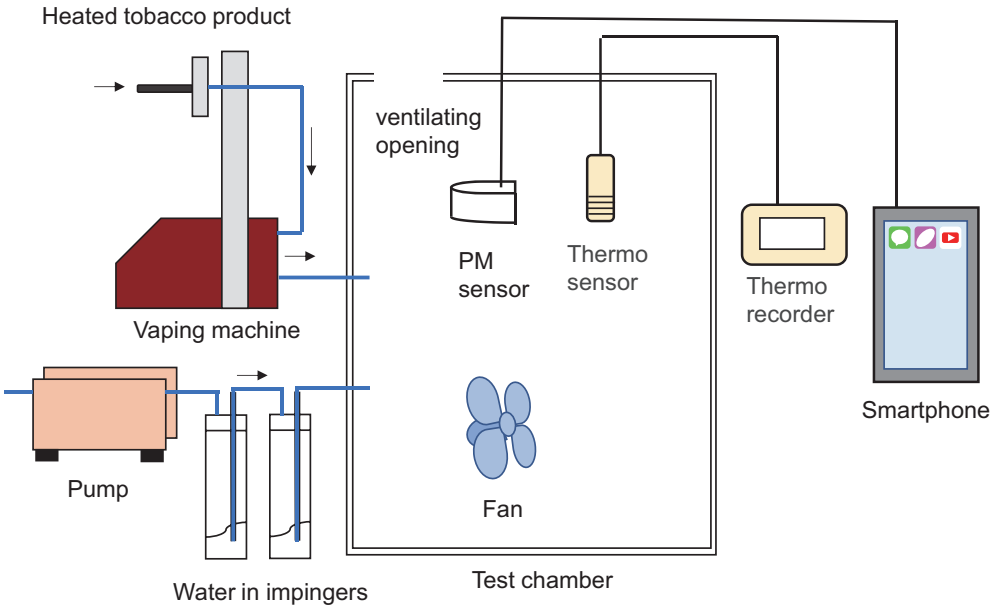

Fig. 1 A schematic representation of the chamber experiment conducted in this study.

2.3 Puffing and environmental condition

The Ploom TECH device was consumed by the Linear Vaping Machine following the International Organization for Standardization (ISO) puffing protocol [11] with a minor modification, consisting of puff duration of 2 s, inter-puff interval of 120 s (originally 60 s), puff volume of 35 mL, puff rate of 1.05 L min^{-1}, and a "Bell" puffing profile. Preliminary tests revealed that the range of

PM concentrations in the chamber exceeded the upper limit of the smartphone air quality monitor during repeated puffing, and thus the inter-puff interval was subsequently extended from 60 s to 120 s. The number of puffs in a single run was set to 10, and three repeat runs were conducted under two conditions: low RH (temp. = 26℃, RH = 29%) and high RH (temp. = 26℃, RH = 83%). Given that the target substance in this study was "aerosol," the vaping device did not incorporate a Cambridge filter that is typically used for the separation of gas and solid phase.

3 Results and Discussion

The time courses of the concentrations of $PM_{2.5}$ and PM_{10} in the test chamber showed similar patterns in three repeated runs. Fig. 2 presents the results obtained for Run #1 under low and high RH conditions as representative of the three runs. In general, the concentrations of both $PM_{2.5}$ and PM_{10} peaked within a few minutes after puffing the Ploom TECH device, and subsequently decreased with time. However, we observed differences in the peak maximum concentrations in puff profiles under the two RH conditions. At low RH, the peak concentrations of $PM_{2.5}$, and PM_{10} were 28 ± 11 μg m^{-3} ($n = 30$) and 38 ± 19 μg m^{-3} ($n = 30$), respectively. Comparatively, the peak concentration of $PM_{2.5}$ and PM_{10} under high RH conditions were 73 ± 19 μg m^{-3} ($n = 30$) and 84 ± 23 μg m^{-3} ($n = 30$), respectively, both values of which were significantly higher than the corresponding values under low RH ($p < 0.05$, t-test). These findings thus indicate that the generated aerosols immediately lost water to reach equilibrium with the moisture content in the chamber, and that the levels of PM in the aerosol are dependent on the environmental RH.

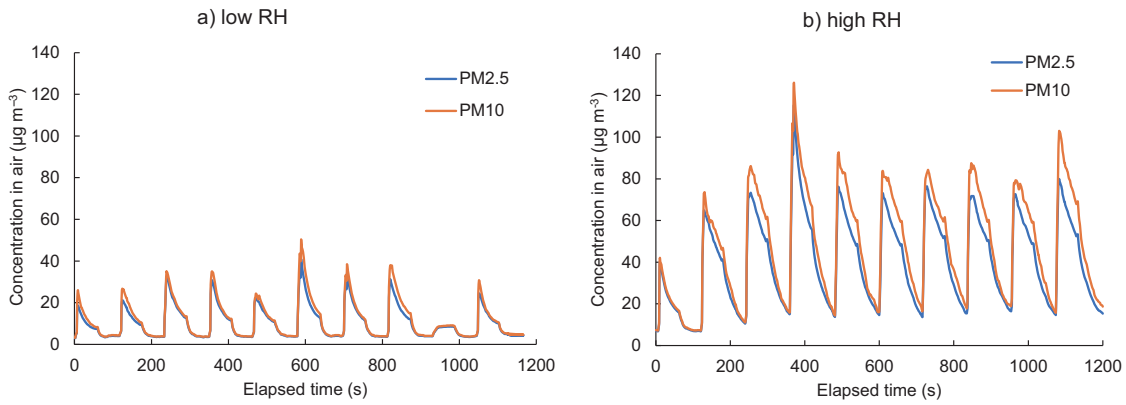

Fig. 2 Typical time-courses of the concentration of $PM_{2.5}$ and PM_{10} in air within the test chamber during a series of 10 puffs of the Ploom TECH device under low RH (temp. = 26℃, RH = 29%) and high RH (temp. = 26℃, RH = 83%) conditions.

Since the $PM_{2.5}$ and PM_{10} concentrations cover the different range of particle size respectively, the concentration ratio ($PM_{10}/PM_{2.5}$) reflects the size distribution of aerosol in the test chamber. Fig. 3 shows typical time-courses of $PM_{10}/PM_{2.5}$ during a series of 10 puffs of Ploom TECH under low RH and high RH conditions (Run#1). Under the low RH condition, the ratio immediately increased just after puffing and decreased within 20 s to the background level. To the contrary, the increase in $PM_{10}/PM_{2.5}$ after puffing was rather moderate under high RH condition. The

$PM_{10}/PM_{2.5}$ at the peaks was observed to range from 1.1 to 2.4, with an average of 1.4 ± 0.38 ($n = 30$) at low RH, whereas at high RH, the ratio ranged from 1.1 to 1.3, with an average of 1.1 ± 0.067 ($n = 30$). The evaporation rate of a water droplet is inversely proportional to its radius [12]; the finer particle has a nature to lose water more easily. The significant difference between these values ($p < 0.01$, t-test) indicates that RH also affects the size distribution of the hygroscopic aerosol at the peaks in the environment.

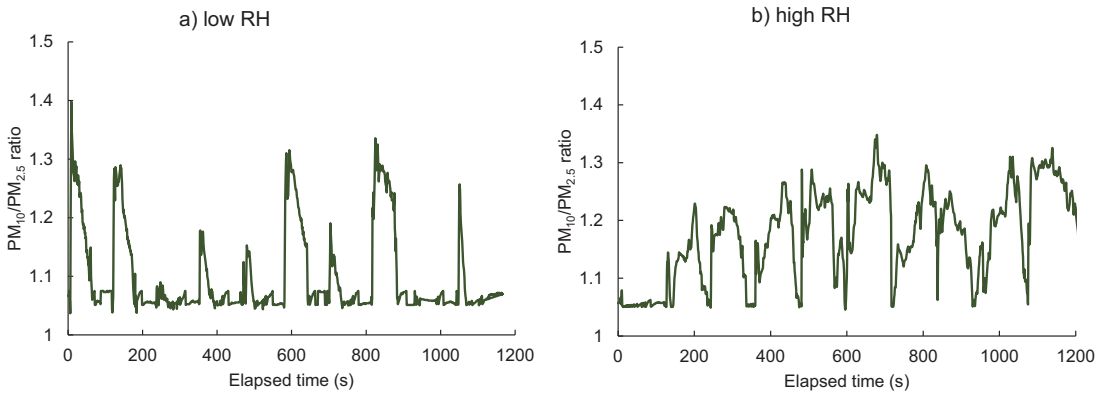

Fig. 3 Typical time-courses of $PM_{10}/PM_{2.5}$ in air of the test chamber during a series of 10 puffs of Ploom TECH under low RH (temp. = 26℃, RH = 29%) and high RH (temp. = 26℃, RH = 83%) conditions.

With regard to the hygroscopic aerosol, we can assume three possible processes whereby the aerosol is removed from the chamber: removal by air exchange, evaporation (loss of water and subsequent volatilization of glycerin and propylene glycol) [7], and deposition on the surface of the chamber. In this context, it should be noted that removal via coagulation was not taken into consideration in the present study, as this process is generally applicable only to finer aerosol of particle size 0.1 μm or less [13]. Accordingly, the change in PM concentration C with time t can be described as follows:

$$\frac{dC}{dt} = -NC - R_{evap} - R_{dep}, \qquad \cdots ①$$

where N is the air exchange rate of the test chamber ($2.2\,h^{-1}$), R_{evap} is the evaporation rate, and R_{dep} is the deposition rate. Fig. 4 shows two linear decay plot generated by log conversion of the time-course PM concentrations. By applying a first-order decay to the first and second phases, the change in PM concentration C with time t can be described using the rate constants k_1 and k_2.

$$\frac{dC}{dt} = -k_1 C - k_2 C \qquad \cdots ②$$

As the air in the test chamber was constantly exchanged during the measurement period, the values obtained for k_1 and k_2 must reflect the air change rate ($N = 2.2\,h^{-1}$). Table 1 shows the k_1 and k_2 values derived from the log C slopes obtained for $PM_{2.5}$ and PM_{10} under low and high RH conditions, excluding some irregular peaks. Given that the values of both $k_1$and k_2 are considerably greater than N, evaporation and deposition are presumed be the dominant processes for the

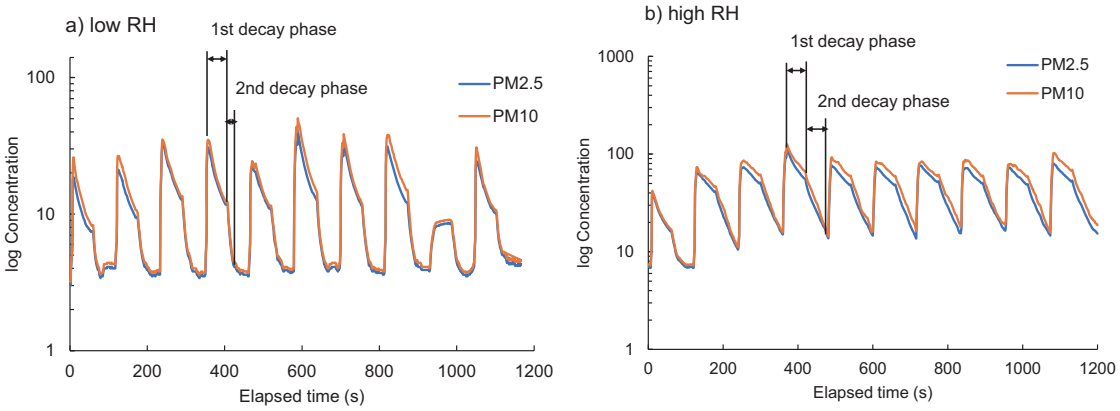

Fig. 4 Typical linear decays plots for the time-courses of $PM_{2.5}$ and PM_{10} concentrations derived from the curves shown in Fig. 2 converted to a log scale. The first and second phases of the 4^{th} puffs are indicated as examples.

decay of hygroscopic aerosols. For both $PM_{2.5}$ and PM_{10}, the k_1 values were lower than those of k_2 under both RH conditions, thereby indicating the operation of a rate-determining process in the first phase, presumably evaporation. Furthermore, higher values of $k_1$and k_2 were observed under high RH conditions, thus indicating that the rate of hygroscopic aerosol decay is also dependent on environmental RH.

Table 1 Apparent first-order decay rate constants derived from the first and second phase slopes for $PM_{2.5}$ and PM_{10} in the test chamber. Number of puffs used for this calculation was 27 for low RH and 30 for high RH conditions.

	$PM_{2.5}$		PM_{10}	
	$k_1(h^{-1})$	$k_2(h^{-1})$	$k_1(h^{-1})$	$k_2(h^{-1})$
Low R.H.	97 ± 45	245 ± 144	99 ± 38	229 ± 118
High R.H.	33 ± 9.4	77 ± 16	30 ± 10	76 ± 18

4 Conclusion

In this study, we aimed to determine the influence of relative humidity on the behavior of aerosols generated from heated tobacco products. Given that aerosols consist of water droplets containing glycerin and propylene glycol, the levels of $PM_{2.5}$ and PM_{10} in air, along with their size distribution and decay rates, were found to be highly dependent on the relative humidity within the test chamber. The findings in this study will also provide a valuable reference for gaining insights into the airborne transmission of novel coronaviruses and other viruses, as such pathogens are potentially present in water droplets in indoor air.

Acknowledgement

This study was conducted as a part of study on *Development of standard test methodology for evaluating chemical hazard of e-cigarette and heat-not-burn tobacco based on aerosol analysis*,

Influence of relative humidity on the behavior of aerosols generated from heated tobacco products supported by Smoking Research Foundation.

References

[1] L. Cancelada, M. Sleiman, X. Tang, M.L. Russell, V.N. Montesinos, M.I. Litter, L.A. Gundel and H. Destaillats, *Heated tobacco products: Volatile emissions and their predicted impact on indoor air quality*, Environ. Sci. Technol., 53(13) (2019), 7866–7876.

[2] S. Uchiyama, M. Noguchi, N. Takagi, H. Hayashida, Y. Inaba, H. Ogura and N. Kunugita, *Simple determination of gaseous and particulate compounds generated from heated tobacco products*, Chem. Res. Toxicol., 31 (7) (2018), 585–593.

[3] K. Bekki, Y. Inaba, S. Uchiyama and N. Kunugita, *Comparison of chemicals in mainstream smoke in heat-not-burn tobacco and combustion cigarettes*, J. UOEH, 39(3) (2017), 201–207.

[4] R. Dusautoir, G. Zarcone, M. Verriele, G. Garçon, I. Fronval, N. Beauval, D. Allorge, V. Riffault, N. Locoge, J. M. L. Guidice and S. Anthérieu, *Comparison of the chemical composition of aerosols from heated tobacco products, electronic cigarettes and tobacco cigarettes and their toxic impacts on the human bronchial epithelial BEAS-2B cells*, J. Hazard Mat., 401(2021), 123417.

[5] N. Nordlund, M. Smith, S. Maeder, T. McGrath, J.P. Schaller, P. Pratte, P. Picavet, M. Peitsch, *Scientific substantiation of the absence of combustion and no smoke formation in the Electrically Heated Tobacco Product (EHTP)*, PMI Science, https://www.pmiscience.com/library/publication/

[6] Y. Sekine and T. Yamamoto, *Physical and chemical property of mainstream aerosol generated from heated tobacco products*, Indoor Environ., 24(2) (2021), 135–144. (in Japanese)

[7] T. Wright, C. Song, S. Sears and M.D. Petters, *Thermodynamic and kinetic behavior of glycerol aerosol*, Aerosol Sci. Tech., 50(12) (2016), 1385–1396.

[8] S. Nakai and A. Oishi, *Actral status of smoking of heat-not-burn tobacco(HNB) and electric cigarettes(e-cig) and measurement methods of particulate matter emitted from HNB or e-cig*, Smoking Research Foundation Annual Report 2020, (2021), 799–803. (in Japanese)

[9] Y. Ishigaki, K. Tanaka, Y. Matsumoto, Y. Y. Maruo and H.A. Pradana, *Citizen sensing for environmental risk communication, action research on $PM_{2.5}$ air quality monitoring in East Asia*, Proc. of Cyber 2017, The 2nd Int. Conference on Cyber-Technologies and Cyber-Systems, Wilmington, IARIA, (2017), 11–12.

[10] Ei Ei Pan Nu Yi, Nay Chi Nway, Win Yu Aung, Thant Z., Thet Hnin Wai, Kyu Kyu Hlaing, Maung C., M. Yagishita, Y. Ishigaki, Tin-Tin Win-Shwe, D. Nakajima and Ohn Mar, *Preliminary monitoring of concentration of particulate matter ($PM_{2.5}$) in seven townships of Yangon City, Myanmar*, Environ. Health Prevent. Med., 23(53) (2018), 1–8.

[11] International Organization for Standardization, ISO Standard 4387, Routine analytical cigarette smoking machine-definitions and standard conditions, fourth ed. (2000).

[12] M. Doi, *Physics of Evaporation and Drying —Evaporation Induced Flow and Structural Formation—*, The Phys. Soc. of Japan, 73(8) (2018), 551–557. (in Japanese)

[13] L. S. Ruzer and N. H. Harley, *"Aerosol handbook, measurement. Dosimetry and health effects"*, CRC Press, Boca Raton, FL, USA, (2005), p623.

編集委員長　CHIEF EDITOR
利根川　昭　Akira Tonegawa

編集委員　EDITORS
桐木　紳　Shin Kiriki
都地　崇恵　Takae Tsuji
松井　泰子　Yasuko Matsui
小林　正弘　Masahiro Kobayashi
藤城　武彦　Takehiko Fujishiro
伊藤　建　Takeru Ito
関根　嘉香　Yoshika Sekine
尾崎　浩司　Hiroshi Ozaki

幹事　SECRETARY
遠藤　雅守　Masamori Endo

Proceedings of the School of Science of Tokai University

第 57 巻

2022 年 3 月 20 日　発行

編集兼発行者　東海大学理学部
神奈川県平塚市北金目 4−1−1
4−1−1 Kitakaname, Hiratsuka-shi, Kanagawa-ken, Japan